P6.20 **PRECIPITATION SIGNATURES IN SSMIS IMAGERY**

F.J. Turk[1] T.F. Lee[1], S.D. Miller[1], R. Ferraro[2], F. Weng[2]
[1]Naval Research Laboratory, Marine Meteorology Division, Monterey, CA USA
[2]NOAA-NESDIS, Office of Research and Applications, Camp Springs, MD USA

1. INTRODUCTION

The launch of DMSP F-16 in October 2003 deployed the first of five planned Special Sensor Microwave Imager Special (SSMIS) passive microwave conically-scanning imagers. Similar to its predecessor SSMI with imaging channels between 19-91 GHz, the SSMIS incorporates a wider swath with co-located imaging and sounding capabilities. The SSMIS includes 7 (6) lower (upper) air temperature sounding channels near the 60 GHz oxygen absorption band, an additional environmental channel at 150 GHz and three 183 GHz mid-to-upper troposphere moisture sounding channels. With its 24 channels, the SSMIS combines the capabilities of the SSMI and the existing Advanced Microwave Sounding Unit (AMSU-B) on a single platform and alleviates the difficulty of aligning scenes from separate conical and cross-track scanning instruments.

The SSMIS sensor combines passive microwave imaging, temperature and moisture soundings into a single conically-scanning radiometer with a near-constant viewing angle. The antenna/calibration subsystem consists of the main reflector, six feedhorns, a warm calibration load and a cold calibration reflector. The main reflector is an offset parabolic reflector and rotates along with the majority of the sensor hardware, at 31.6 revolutions per minute. Channels 1-7 sense in the 50-60 GHz range providing radiometric information sufficient to resolve lower atmospheric temperature at standard levels between 1000-10 hPa. Upper atmospheric temperature sounding extending into the mesosphere up to 0.02 hPa (80-km) is made possible by channels 19-24.

SSMIS imaging channels similar in resolution and spectral frequency to the SSMI (91 GHz on SSMIS vs. 85 GHz on SSMI) are provided between channels 12-18. Channels 8 is a imaging channel centered at 150 GHz and channels 9-11 are three humidity profiling channels centered about 183.31 GHz, maintaining continuity with similar capabilities on the AMSU-B instrument. This paper shows examples of 150 and 183 GHz SSMIS imagery over tropical precipitation, and also snowfalling storms where fast moving, cold frontal based rain systems and complex land surface features present difficulties to current algorithms. Comparisons will be shown with near coincident DMSP F-15 SSMI data, which follows just behind the F-16 orbit pattern, as well as AMSU-B data from NOAA-15.

2. SSMIS AND RAINFALL

An example F-15 DMSP SSMI 85H GHz image from an overpass of Hurricane Katrina on 29 August 2005 at 1514 UTC is shown in Figure 1, as the storm made landfall near the Louisiana-Mississippi coastal border. For comparison, the 91H GHz channel image from the F-16 SSMIS is shown in Figure 2, approximately 30 minutes earlier. The shift in the convection owing to the storm motion is evident, as is the slightly cooler background T_B owing to the increased atmospheric water vapor absorption at 91 GHz vs. 85 GHz. The ~20 K land-water TB difference is due to the radiometrically colder ocean surface observable in this window band.

The 150 GHz image of Figure 3 shows that the increased atmospheric water vapor absorption at this frequency has masked the land-ocean background differences, and the clearsky background T_B has essentially saturated near 285 K. Regions of convection are radiometrically colder at this frequency than at 91 GHz owing to the increased scattering coefficient of precipitation-sized ice particles (Weng et. al, 2003). Therefore, a major advantage of this channel is its potential to consolidate precipitation retrievals near and across coastlines, where the spaceborne passive microwave radiometer field-of-view (FOV) contains fractional coverage from both over-land and over-ocean. This often leads to a “ribboning effect” noted along coastlines when lower-frequency channels are used in the retrieval (i.e., light rain is falsely identified along the trace of the coastal boundary under non-

---

[1] Corresponding author address: Francis J. Turk, Naval Research Laboratory, Marine Meteorology Division, 7 Grace Hopper Ave., Monterey, CA 93943, Tel: (831)-656-4888, Email: turk@nrlmry.navy.mil.

precipitating conditions, producing the visual effect of a ribbon). Comparison with the NEXRAD radar coverage from three hours earlier (Figure 4) illustrates the connection between the 150 GHz TB < 190 K and reflectivities > 30 dBZ. The magnitude of the 150 GHz precipitation scattering signal is largely dependent upon the size distribution and density of the ice hydrometeors and their location within the vertical moisture column, with shape and orientation being of secondary importance (Bauer and Mugnai, 2004).

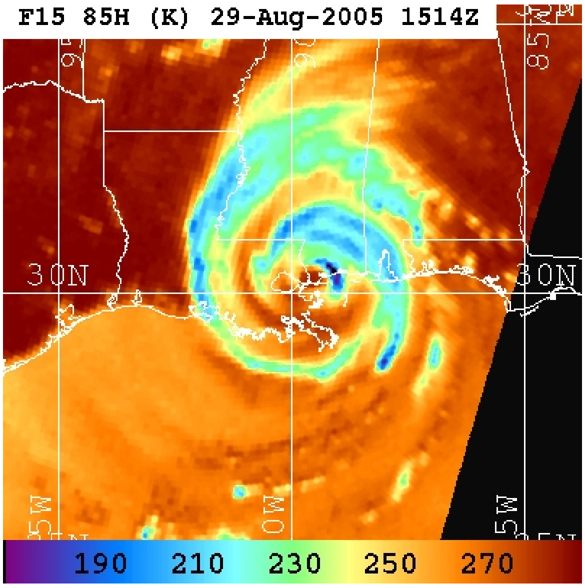

Figure 1. SSMI 85H channel imagery (Kelvin units) from DMSP F-15 overpass on 29 August 2005 at 1514 UTC.

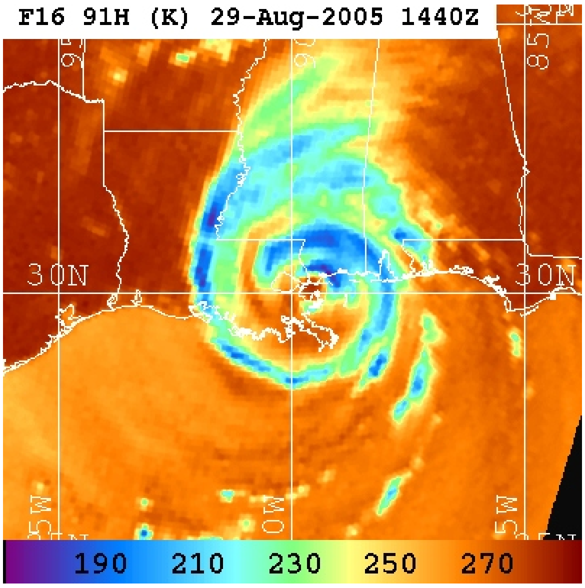

Figure 2. SSMIS 91H (channel 18) imagery (Kelvin units) from DMSP F-16 overpass on 29 August 2005 at 1440 UTC.

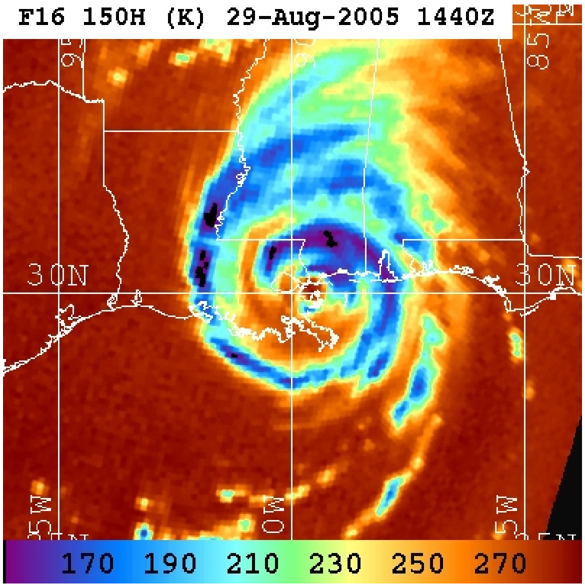

Figure 3. Same as Figure 2, but SSMIS 150H (channel 8) imagery.

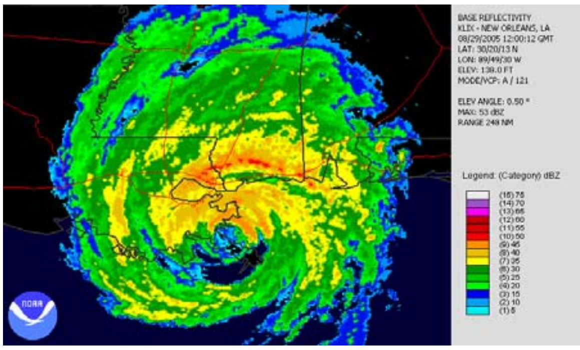

Figure 4. NEXRAD PPI reflectivity radar scan from 1200 UTC on 29 August 2005. NEXRADA data and figure courtesy of the NOAA National Climate Data Center (NCDC) at http://www.ncdc.noaa.gov/oa/climate/research/2005/katrina.html.

Figure 5-7 depict the three 183.31 GHz-centered moisture sounding channels on the SSMIS, which under non-cloudy skies sense at progressively higher levels (colder T_B) in the troposphere (i.e, 183.31±1 < 183.31±7), forming the basis of moisture profile retrievals. Under cloudy conditions, the scattering and absorption properties of the hydrometeor column are superimposed upon the vertical moisture profile. However, if the precipitation-sized ice column rises to a high enough level through cloud vertical development, the satellite-observed T_B can be radiometrically cooler (due to ice hydrometeors scattering the upwelling radiation away from the sensor) than the surrounding environment, even at the uppermost 183.31±1 channel. Figure 7 shows this effect (green-blue colors < 230 K). Intuitively, there should be some visual similarity between the structure of the coldest TB in this channel and with the coldest cloud tops as revealed in longwave infrared cloud imagery. Figure 8 shows the GOES-12 11 µm (channel 4) imagery five minutes later at 1445 UTC.

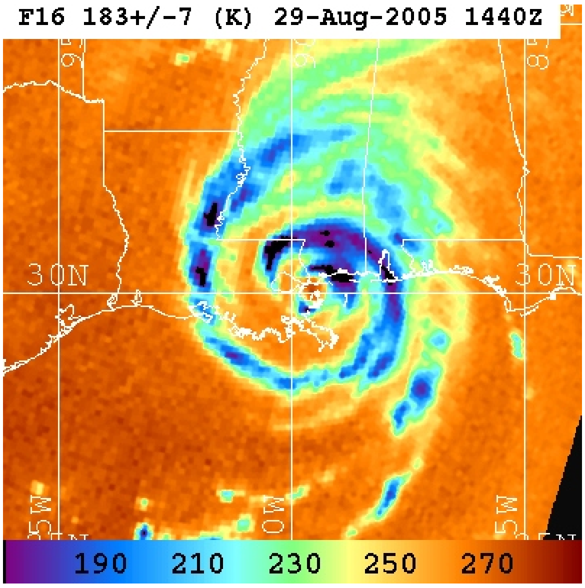

Figure 5. Same as Figure 2, but SSMIS 183.31 ± 6.6 GHz (channel 9) imagery.

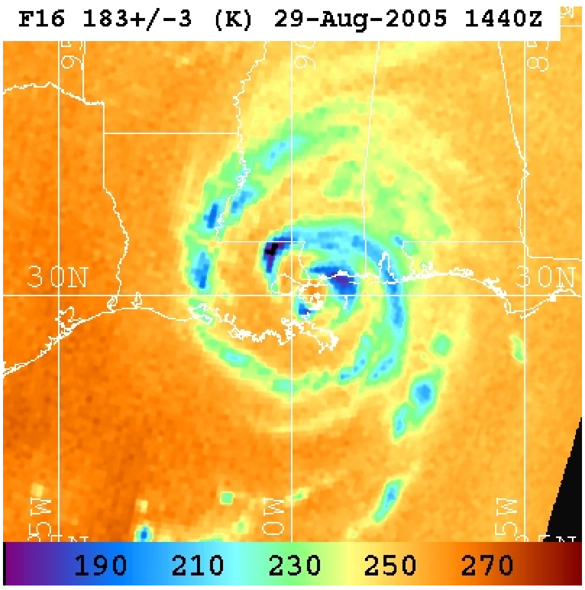

Figure 6. Same as Figure 2, but SSMIS 183.31 ± 3 GHz (channel 10) imagery.

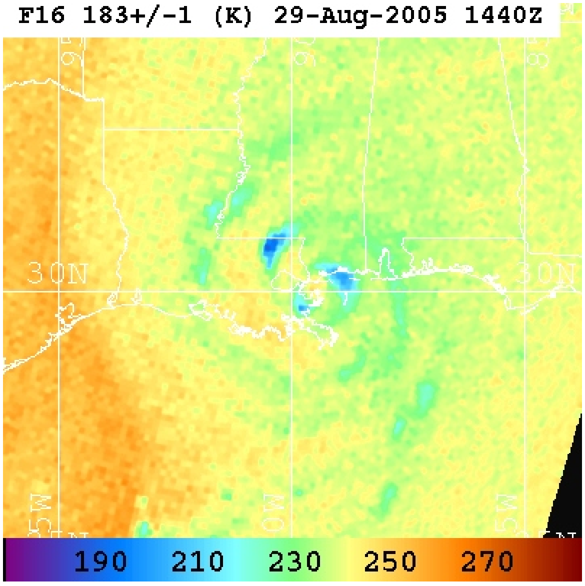

Figure 7. Same as Figure 2, but SSMIS 183.31 ± 1 GHz (channel 11) imagery.

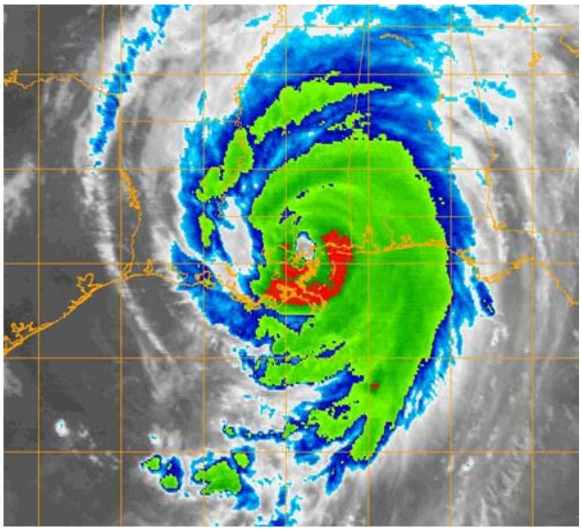

Figure 8. GOES-12 channel 4 (11 µm) imagery from the 1445 UTC sector scan on 29 August 2005.

At 183.31±7 GHz, the troposphere is more transparent and the channel senses deeper into the convective cloud. Here, ice scattering proceeses are less attenuated by the atmospheric water vapor (which through path absorption tends to lower the effective albedo owing to the ice alone). Over cloud systems covered with precipitation-sized ice, the enhanced scattering properties within this band can lead to instances where T_B(183.31±7) < T_B(183.31±1). For deep convective situations, the difference can fall below -60 K as depicted in Figure 9, where the difference between the

183.31±7 and 183.31±1 channels is shown. Note the similarity of the structure between this figure and Figure 3 (the 150 GHz SSMIS image).

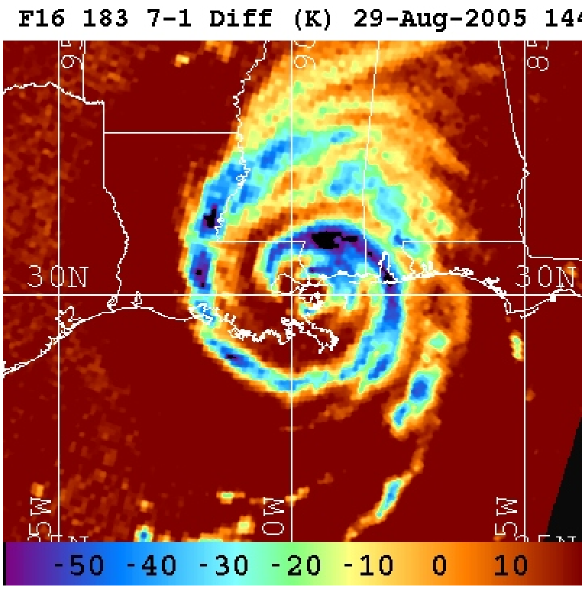

Figure 9. SSMIS image depicting the brightness temperature difference between Figures 5 (183.31±6.6 GHz channel) and Figure 7 (183.31±1 GHz channel).

While the land-ocean background is obscured at 150 GHz for moist tropical environments, the surface emission contribution may not be totally opaque over drier middle/high-latitude atmospheres or during the winter months (Skofronick-Jackson et. al, 2004). Lighter rainrates, which form a greater percentage of higher latitude precipitation, may lack a deep enough ice canopy to produce a significant scattering signal. For snow covered surfaces, the surface emissivity can be highly variable, depending on snow age and grain size. The signal may also be terrain dependent (terrain changes the viewing angle, WHAT ABOUT LOOK-ANGLE EMISSIVITY DEPENDENCE AND VARIABLE EMISSIVITY AS A FUNCITON OF SOIL MOISTURE?). Nonetheless the addition of the 150 and 183 GHz capability will extend the capability of precipitation sensing over many situations that are problematic for SSMI-like sensors.

3. SSMIS AND SNOWFALL

The 150 and 183 GHz channels of the across-tracking scanning AMSU-B instruments onboard the NOAA series of satellites (since NOAA-15, continuing with the Microwave Humidity Sounder on NOAA-18) have been examined for their use in snowfall detection over land (Kongoli et.al. 2003; Skofronick-Jackson et.al, 2004; Chen and Staelin, 2003). As with the previous example of Hurricane Katrina, the use of higher frequencies at 150 and 183 GHz effectively screens the surface emission (passive microwave T_B measured at frequencies less than than 37 GHz is highly variable over snow-covered surfaces). For a given ice water path, the T_B depression at 150 GHz is larger than at 90 GHz (wider dynamic range) and the sensitivity of these frequencies to precipitating ice has been examined by Bennartz and Bauer (2003) and Bauer and Mugnai (2004).

To demonstrate the potential of the SSMIS for improving snowfall identification over land, SSMIS 91H channel imagery from a DMSP F-16 overpass on 10 October 2005 at 1549 UTC is shown in Figure 10, centered over the state of Colorado. An early season snowstorm descended from the north across the eastern front range of the state, with the greatest snowfall accumulations recorded to the south and east of Denver and also in the higher elevations to the west. The areas with the coldest 150 GHz scattering-based T_B depressions are near 220 K in north-central Colorado (Figure 10). For comparison, the AMSU-B 89 GHz imagery from the NOAA-15 overpass approximately two hours earlier is shown in Figure 11. The on-Earth resolution of the AMSU-B ranges from 15-km (slightly worse than SSMIS 91 GHz) near subpoint to 50-km at swath edges and nearby pixel averaging has been done to preserve image continuity across the swath (artifacts are still evident in the lower right of Figure 11), which smoothes out the features compared to Figure 10. In addition, the limb darkening (larger water vapour paths at higher scan angles) across the scan makes quantitative comparison with the conically-scanning SSMIS difficult. Figures 12 and 13 show the associated difference between the 150 GHz channels.

To verify that these scattering depressions were indeed associated with snowfall, we refer to Figure 14 which shows a cloud/snow enhancement (Miller et. al, 2005) generated from the MODIS radiometer onboard the EOS-Aqua afternoon overpass (1330 local time) on 11 October (the following day, when the main storm complex had passed and clouds had begun to clear). This simple enhancement is based on differences between cloud and snow properties in the optical spectrum (visible, near infrared and thermal infrared). Within this image, green is associated with clear sky land background, yellow is low cloud, pink/orange is high cloud, and white/blue is snowcover. Although some of the snow to the eastern half of Colorado remains obscured by low clouds, the placement of the snowfall noted in the center of the image and in the mountains southwest of Denver is in general accord with the structure of the 91 and 150 GHz SSMIS imagery from the snowfall event during the morning of the previous day.

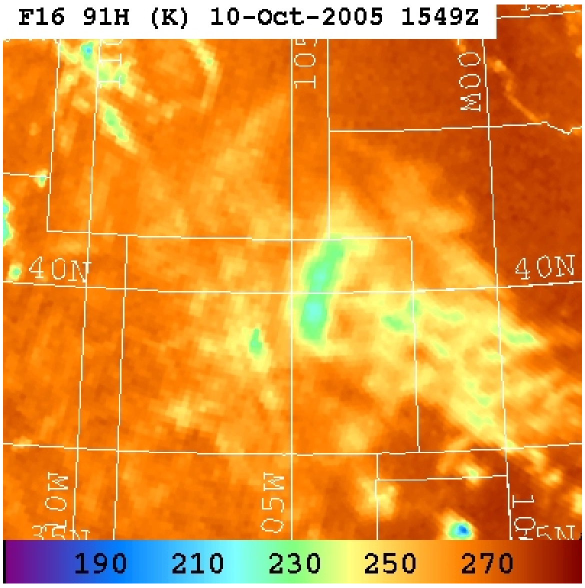

Figure 10. SSMIS 91H channel imagery (Kelvin units) from DMSP F-16 overpass on 10 October 2005 at 1549 UTC. The image is centered over the state of Colorado in the US.

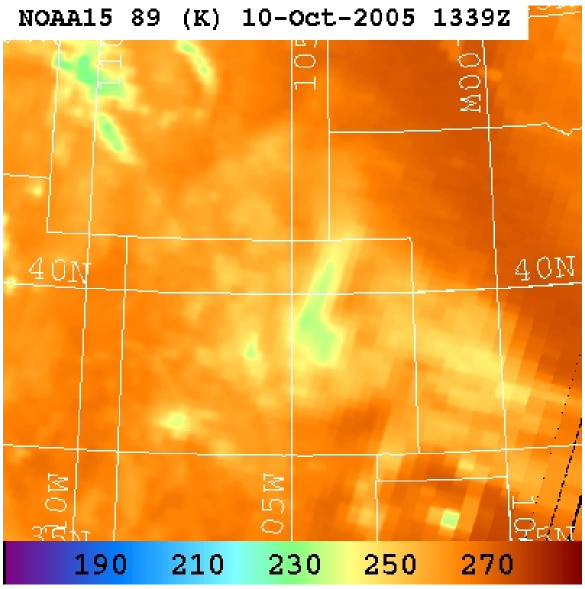

Figure 11. AMSU-B 89 channel imagery (Kelvin units) from NOAA-15 overpass on 10 October 2005 at 1339 UTC.

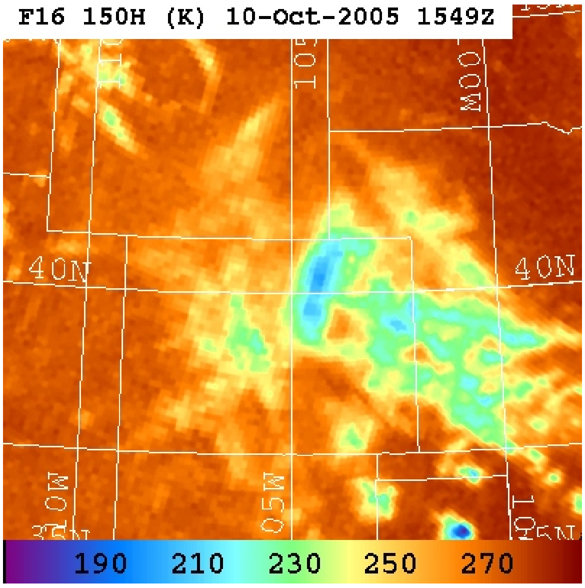

Figure 12. Same as Figure 10, but for the 150H GHz channel on SSMIS.

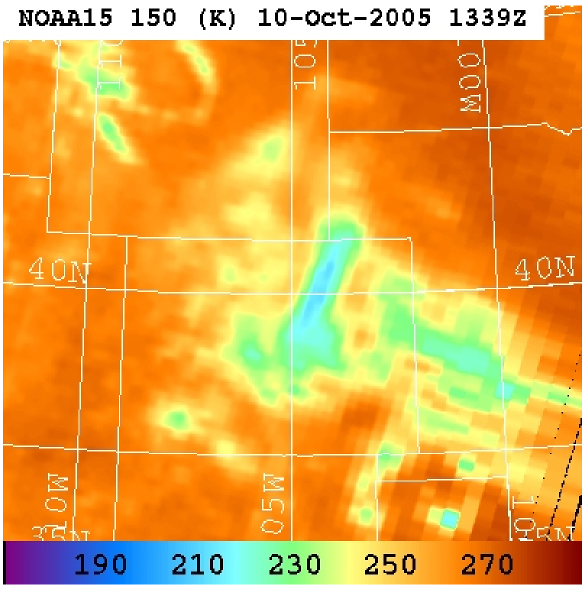

Figure 13. Same as Figure 11, but for the 150 GHz channel on the AMSU-B.

Figure 15 shows the 183.31±1 channel (note the color scale range has been contracted to cover 220-280 K), where the scattering-induced T_B depressions owing to the snow hydrometeors fall only to about 230 K. In the tropical environment associated with the Hurricane Katrina overpass depicted in Figure 9, the difference between the 183.31±7 and 183.31±1 channels was noted to fall below -60 K for the regions of deepest convection. For this snowfall situation, Figure 16 shows that this same 183 GHz T_B difference only falls to about -15 K, owing to smaller sized ice particles and lower density, providing overall

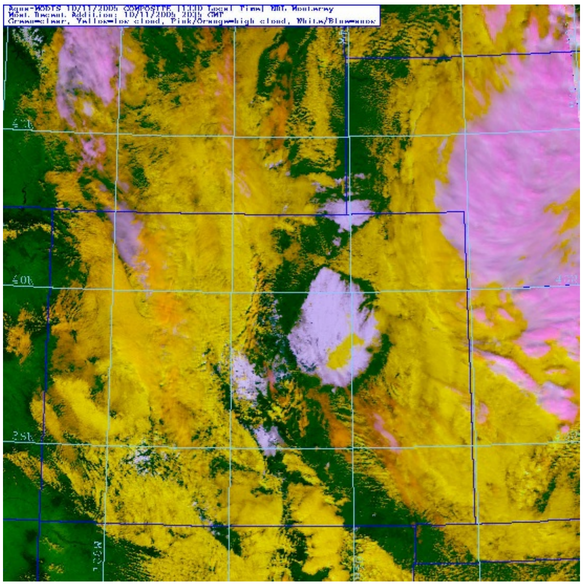

Figure 14. Multispectral MODIS cloud/snow enhancement from the afternoon (1330 local time) EOS-Aqua overpass on 11 October 2005, the day after the snow event. Green is associated with clear skies, yellow is low cloud, pink/orange is high cloud, and white/blue is snow cover (Miller et. al, 2005).

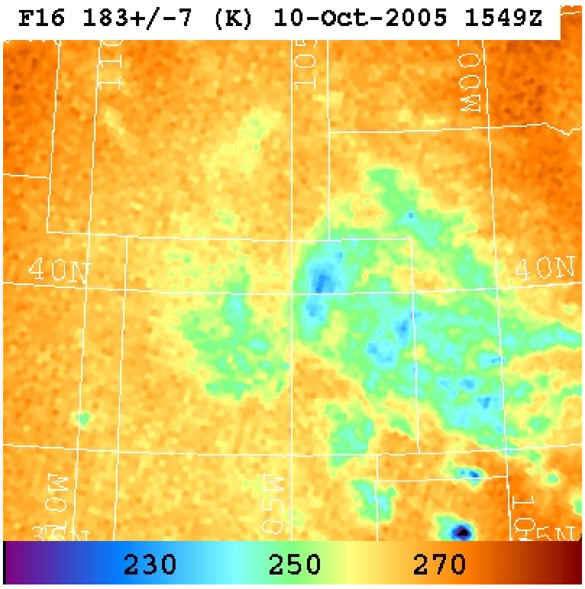

Figure 15. Same as Figure 10, but SSMIS 183.31 ± 6.6 GHz (channel 9) imagery.

weaker ice scattering properties. A full explanation of this type of T_B pattern and behavior requires polarimetric radiative transfer models and size and shape parameterizations (Kim et. al, 2004), and is beyond the scope of this discussion. Additionally, if the snowfall event occurs during extreme cold and dry conditions, then the ice scattering T_B depression may not be sufficient to drop below the cold land surface radiometric temperature (i.e, the retrieval would fail in this case). However, the encouraging results developed so far for the AMSU-B snowfall techniques are likely to be improved with the finer scale and conically-scanning capabilities provided by the SSMIS.

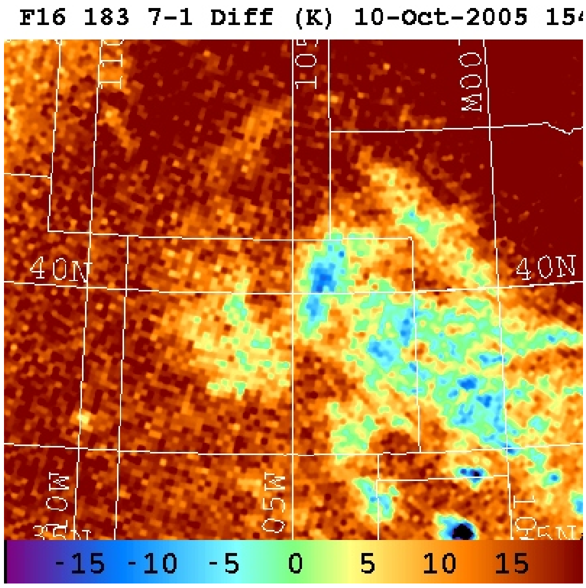

Figure 16. SSMIS image depicting the brightness temperature difference between Figures 5 (183.31±6.6 GHz channel) and Figure 7 (183.31±1 GHz channel).

4. CONCLUSIONS

We have shown examples from the first (DMSP F-16) of the Special Sensor Microwave Imager Special (SSMIS) passive micrrowave imager/sounders. SSMIS imagery at 91, 150, and 183 GHz was shown from overpasses of two types of events, a moist environment tropical hurricane with associated deep convection, and a drier, colder middle latitude snowfall event. As has been shown earlier by several authors with AMSU-B datasets, the 150 GHz and 183 GHz capabilities of the SSMIS have the capability to improving the identification and quantification of regions of snowfall. A full characterization of this capability requires radiative transfer modeling of typical snow-producing cloud structures and representative ambient temperature and moisture conditions. Additional observations from cloud radars, such as the planned CloudSat mission (Stephens et. al., 2002) have the capability to analyze the vertical profile of the snow structure. The International Precipitation Working Group Ongoing is coordinating ongoing research in this area, and recently sponsored a snowfall modeling workshop (IPWG; Turk and Bauer, 2005). More information on this workshop is available on the IPWG website at http://www.isac.cnr.it/~ipwg. We conclude by mentioning that a similar channel combination will be available from the Conically Scanning Microwave Imager Sounder (CMIS) instrument during the National Polar Orbiting Environmental Satellite System (NPOESS) era and a high frequency option has been approved for the Global Precipitation Mission (GPM) Microwave Imager (GMI) later this decade.

ACKNOWLEDGMENTS

The first three authors acknowledge the support of the research sponsors, the Office of Naval Research, Program Element (PE-0602435N) and the the Oceanographer of the Navy through the program office at the Space and Naval Warfare Systems Command, SPAWAR PEO C4I&Space/PMW-180 (PE-0603207N). The first author also acknowledges support from the National Aeronautics and Space Administration Earth-Sun Exploration Division under grant NNG04HK11I. We thank Steve Swadley and Gene Poe for their thorough efforts in leading the SSMIS Cal/Val program and for their suggestions with data interpretation.

REFERENCES

Bauer, P. and A. Mugnai, 2004: Precipitation profile retrievals using temperature-sounding microwave observations. *J. Geophys. Res*., **108** D23, 4730, doi:10.1029/2003JD003572.

Bennartz, R. and P. Bauer, 2003: Sensitivity of microwave radiances at 85-183 GHz to precipitating ice particles. Radio Science, 38, 4, 8075, doi: 10.1029/2002RS002626

Chen, F.W., and D.H. Staelin, 2003: AIRS/AMSU/HSB precipitation estimates, *IEEE Trans. Geosci. Rem. Sens.*, **41**, 410-417.

Kim, M.-J., G. Skofronick-Jackson, and J. A. Weinman, 2004: Intercomparison of millimeter wave radiation transfer models. *IEEE Trans. Geosci. Remote Sensing,* **42**, No.9, 1882-1890.
Kongoli C., P. Pellegrino, R. R. Ferraro, N.C. Grody, and H. Meng, 2003: A new snowfall detection algorithm over land using measurements from the AMSU, *Geophys. Res. Let.*, **30**,1756-1759.

Miller, S. D., T. F. Lee, and R. Fennimore, 2005: Satellite-based daytime imagery techniques for snow cover and cloud delineation, J. Appl. Meteorol., 44(7), 987-997.

Skofronick-Jackson, G.M., M.J. Kim, J.A. Weinman, D.E. Chang, 2004: A physical model to determine snowfall over land by microwave radiometry. *IEEE Trans. Geosci. Rem. Sens*., **42**, 1047-1058.

Stephens, G.L., Deborah G. Vane, Ronald J. Boain, Gerald G. Mace, Kenneth Sassen, Zhien Wang, Anthony J. Illingworth, Ewan J. O'Connor, William B. Rossow, Stephen L. Durden, Steven D. Miller, Richard T. Austin,Angela Benedetti,Cristian Mitrescu and the CloudSat Science Team, 2002: The CloudSat Mission and the A-Train**.** *Bulletin of the American Meteorological Society*, **83**, No. 12, 1771–1790.

Turk, F.J and P. Bauer, 2005: Proc. 2nd International Precipitation Working Group, 25-28 October, Monterey, 355 pp. Available from EUMETSAT, Am Kavalleriesand 31, D-64295 Darmstadt, Germany, EUM P.44, ISBN 92-9110-070-6. Online at http://www.isac.cnr.it/~ipwg.

Weng, F., L. Zhao, G. Poe, R. Ferraro, X. Li and N. Grody, AMSU cloud and precipitation algorithms, *Radio Science*, **38(4)**, 8068-8079, 2003.